Designing Hand-Immune Handset Antennas With Adaptive Excitation and Characteristic Modes

Rasmus Luomaniemi, *Graduate Student Member, IEEE*, Pasi Ylä-Oijala, Anu Lehtovuori, and Ville Viikari, *Senior Member, IEEE*

Abstract—This article presents a design process for a hand-immune mobile antenna system. Characteristic modes (CMs) of a mobile phone and hand combination are analyzed to find the desired modes with good radiation properties. The efficient excitation of these modes is implemented by utilizing the antenna cluster technique. The proposed mobile antenna design has a small ground clearance of only 2 mm and can cover the 700–960 MHz low band, 1700–2700 MHz middle-high band (MHB) with two multiple-input–multiple-output (MIMO) antennas, and the 3300–3800 MHz high band with four MIMO antennas. The measurement results confirm that the proposed CM analysis-based design method in a realistic use case leads to a robust antenna design with competitive performance.

Index Terms—Characteristic mode analysis (CMA), mobile handset antennas, multiple-input–multiple-output (MIMO) antennas, user effect.

I. Introduction

ONE of the largest problems in modern mobile antenna design is to achieve good performance with the user holding the device. With increasing demand for new and wider frequency bands and constantly decreasing volume available for the antennas, it is difficult to achieve good performance even in free-space conditions. Plenty of research has been carried out to study how the negative effects of the user can be reduced [1]. In this article, we introduce an antenna design process where the user effect is considered in each design step. As a result, we propose a hand-immune mobile antenna design.

Characteristic mode analysis (CMA) has been shown to be a powerful tool for the analysis and design of different types of antennas [2]. A large number of CMA-based antenna designs have been published for a variety of different applications, including mobile antennas, base station antennas, laptop antennas, and wearable antennas (see [3]–[15]). The most common ways of utilizing CMA in antenna design

include excitation of orthogonal modes for good multiple-input–multiple-output (MIMO) performance [16], [17] and combining multiple modes to be excited simultaneously for increased bandwidth [9], [18].

In most CMA-based design scenarios, the antenna is designed in free space neglecting the user effect completely. The effect of the user on the antenna performance is normally only verified with simulations and measurements. Since the user typically has a very strong negative effect on the efficiency of an antenna, there is no guarantee that this approach leads to an optimal design nor even to a satisfactory one. In [19], it has been shown that CMA-based designs suffer from higher absorption losses compared with conventional antenna designs, but they can outperform in terms of correlation and multiplexing efficiency. Therefore, to obtain optimal performance with the user, the CMA model should include both the antenna and the user.

Applying CMA for lossy dielectric structures, however, is not trivial. The generalized eigenvalue equation, used to find the characteristic eigenvalues and eigenvectors (eigencurrents), needs to be defined properly to guarantee that the obtained eigensolutions are useful and physically meaningful completely excluding nonphysical, so-called spurious solutions. This is particularly important for bodies having high dielectric constant and being also highly lossy, such as the human body [20]. Recently, we have shown that CMA can be reliably applied for the analysis of combined PEC (antenna) and lossy dielectric (user) structures [21]. The obtained eigensolutions provide separation of the loss and radiation power, thus allowing simultaneous study of the radiation properties and loss mechanism of the structure.

The antenna cluster technique [22], [23], where several active antenna elements are used collaboratively, is a promising technique for mobile antennas. The combined operation of several active antenna feeds weighted with proper amplitude and phase coefficients provides more adaptivity and better control over the excited characteristic modes (CMs) compared with traditional techniques. In [24], it has been shown that the antenna cluster technique can be used to effectively excite CMs of a metal-rimmed device. Due to the distributed feeding and the possibility to adjust the feeding weights differently for use in free space and with the user, the cluster technique can also be used to reduce the user effect even with antenna designs that have not been originally designed to take this into account [25], [26].

In this article, we combine these two techniques to design hand-immune mobile antennas. The main novelty in our approach is that, for the first time to the author's knowledge, the user's hand is considered in the CMA from the beginning of the design process. By using a broken metal rim with properly designed sections, we can create several resonating modes with good radiation properties in the low-band (LB) frequencies. By designing a multielement feeding arrangement utilizing the antenna cluster technique, we can excite the optimum combination of these modes across wide frequency bands. As a result, a novel antenna design with a significantly reduced user effect is proposed. The proposed design can cover the 0.7–0.96 GHz LB, 1.7–2.7 GHz middle-high band (MHB), and the 3.3–3.8 GHz high band (HB) with one, two, and four antennas, respectively, and achieve equally good performance with the user's hand as in free space.

II. CMA WITH THE USER

CMA is applied to design the LB antenna utilizing the antenna cluster technique. An essential part of the analysis is the proper modeling of losses caused by the human hand. Therefore, we begin by shortly introducing the theoretical background of the applied CMA method. More details of the method can be found in [21]. Other types of CMA formulations for combined PEC and dielectric structures are introduced, e.g., in [27].

A. Theoretical Background and Design Parameters

Let us consider a radiation problem where the structure consists of a metallic PEC structure and a lossy dielectric body. The dielectric part is assumed to be homogeneous with constant complex frequency-dependent permittivity. Let S_C denote the surface of the PEC part and S_D denote the surface of the dielectric one. Assume that $\mathcal{L}$ is a surface integral operator that can be used to formulate the problem in the following generic form:

$$\mathcal{L}[A] = -A^i \tag{1}$$

where A is an unknown current density on the surface of the structure, including both S_C and S_D, and A^i is a given incident field or excitation.

CMA is based on the solutions of a generalized eigenvalue equation [27], [28]

$$\mathcal{L}[A_n] = (1 + j\lambda_n)\mathcal{M}[A_n] \tag{2}$$

where $\mathcal{L}$ is the same integral operator as in (1), $\mathcal{M}$ is a weighting operator to be chosen, λ_n is an eigenvalue, and A_n is the corresponding eigenvector or the eigencurrent.

The main point in the CMA of lossy structures is the proper choice of $\mathcal{M}$ so that the obtained eigensolutions are physically meaningful. For a given operator $\mathcal{L}$, operator $\mathcal{M}$ should be defined so that the eigensolutions are related to radiated fields. This guarantees that the far fields of the modes are orthogonal and the complex-valued eigenvalues λ_n have the following physical interpretation: [20], [21]

$$\text{Re}(\lambda_n) = \frac{P_n^{\text{reac}}}{P_n^{\text{rad}}}, \quad \text{Im}(\lambda_n) = \frac{P_n^{\text{loss}}}{P_n^{\text{rad}}} \tag{3}$$

where P_n^{rad}, P_n^{reac}, and P_n^{loss} are radiated, reactive (stored in the near field), and loss power of a mode, respectively. Since losses contribute only to the imaginary part of the eigenvalues, while the reactive power contributes to the real part, this formulation allows the separation of the loss power from the reactive one.

Once the eigenvalues and eigenvectors are available, they can be used to expand a solution for a scattering or radiation problem (1) as [29]

$$A \approx \sum_n c_n A_n \tag{4}$$

where

$$c_n = -\frac{\int_S B_n \cdot A^i \, dS}{1 + j\lambda_n} \tag{5}$$

with properly normalized eigenvectors A_n and B_n [29]. Here, S is the exterior surface of the structure, including both the PEC and dielectric parts, and A_n and B_n are the eigenvectors of the original eigenvalue equation (2) and the adjoint one written with the adjoints of the operators $\mathcal{L}$ and $\mathcal{M}$, respectively. For self-adjoint integral operators (Hermitian matrices), vectors A_n and B_n agree and modal expansion (4) reduces to the conventional one introduced in [28]. For matrix equations, the eigenvectors of the adjoint equation correspond to the left eigenvectors of the original equation [27], [29].

The following parameters are utilized in the study of the CMs and their properties. In expansion (5), the denominator includes term $1 + j\lambda_n$, similarly as in the corresponding expansion for PEC structures [2], [28]. Hence, the modal significance for lossy structures can be defined similarly as for PEC structures

$$\sigma_n = \frac{1}{|1 + j\lambda_n|}. \tag{6}$$

Since in the lossy case λ_n is complex, σ_n does not reach value one at the resonance, as in the lossless case.

The modal efficiency (the highest obtainable radiation efficiency with mode n) is defined as [21]

$$\eta_n = \frac{1}{1 + \text{Im}(\lambda_n)} = \frac{P_n^{\text{rad}}}{P_n^{\text{rad}} + P_n^{\text{loss}}}. \tag{7}$$

If η_n is close to one, a mode n contributes mostly on radiation. As η_n approaches zero, the mode is poor radiator or the losses dominate.

A third useful parameter for combined PEC and dielectric structures is the modal coupling parameter introduced in [21]

$$\kappa_n = \frac{\text{Re}(\eta_{02}) \int_{S_D} \|J_n\|^2 \, dS + \frac{1}{\text{Re}(\eta_{02})} \int_{S_D} \|M_n\|^2 \, dS}{\text{Re}(\eta_{01}) \int_{S_C} \|J_n\|^2 \, dS} \tag{8}$$

where η_{01} and η_{02} are the wave impedances of the background and the dielectric object, respectively, and J_n and M_n are the electric and magnetic current densities of mode n, respectively. The modal coupling parameter κ_n defines the ratio of the modal currents on the dielectric part and on the PEC part. Equally strong currents on the PEC and the dielectric appear as κ_n is one and values smaller than one mean that the currents on the PEC dominate over the currents on the dielectric.
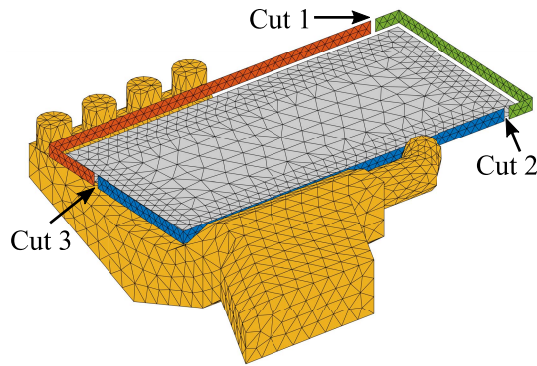
Fig. 1. Antenna structure consisting of a ground plane and a broken metal rim with the hand model.

Fig. 2. Modal significances of 20 modes for the antenna structure of Fig. 1 without the hand.

In the following, the numerical CMA results are computed using an in-house code. Antenna S-parameters, efficiencies, and other related results are simulated with CST Microwave Studio.

B. Metal-Rim Antenna in Free Space

The theory is first applied to a rectangular 146×71 mm^2 PEC plate in free space. The size of the plate is roughly the size of the display panel of current mobile phones. A rectangular plate of this size, used here as a model for the antenna ground plane, supports only a single resonating mode at frequencies below 1 GHz. In our case, the resonance of the first mode appears roughly at 900 MHz. This simple structure has a couple of major design challenges. First, it is difficult to obtain a broadband operation with a single mode. Second, reducing the user effect may be impossible without significant geometrical modifications to the design. Modifications of the ground plane are not allowed in practical designs leaving no means to improve the bandwidth or decrease the user effect.

To gain more freedom for the design parameters, we add a metallic rim around the ground plane. A $150 \times 75 \times 5$ mm^3 continuous rim generates two additional modes that both resonate near the same frequency. By breaking the rim into pieces with appropriate length, we can tune the modes to resonate in the desired frequency range. In addition, the number of cuts in the rim is kept as small as possible. Therefore, the rim is divided into three parts, as shown in Fig. 1: two L-shaped arms along the long edges of the ground plane and a smaller U-shaped section at one end of the ground plane. This allows us to have two sections with appropriate size for LB operation, whereas the shortest section can later be used for higher frequencies. The number of cuts in the rim can be kept small and cuts along the long sides, which could cause problems when covered by the user's hand, can be avoided.

We continue by performing the CMA for the metallic rim antenna structure without the hand. The modal significances of 20 modes with the smallest eigenvalues at the lowest frequency are shown in Fig. 2. Six most significant modes are labeled as, B1, ..., B6, and illustrated with colors. We observe three resonances (maxima of σ_n) at 770 MHz (mode B1), 885 MHz (mode B3), and 900 MHz (mode B2).

Fig. 3 shows the electric currents of modes B1, B2, and B3 at their resonance frequencies. Modes B1 and B3 are rim
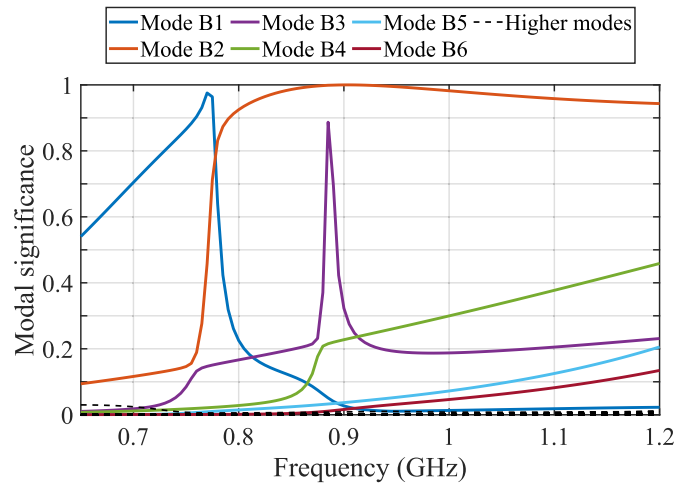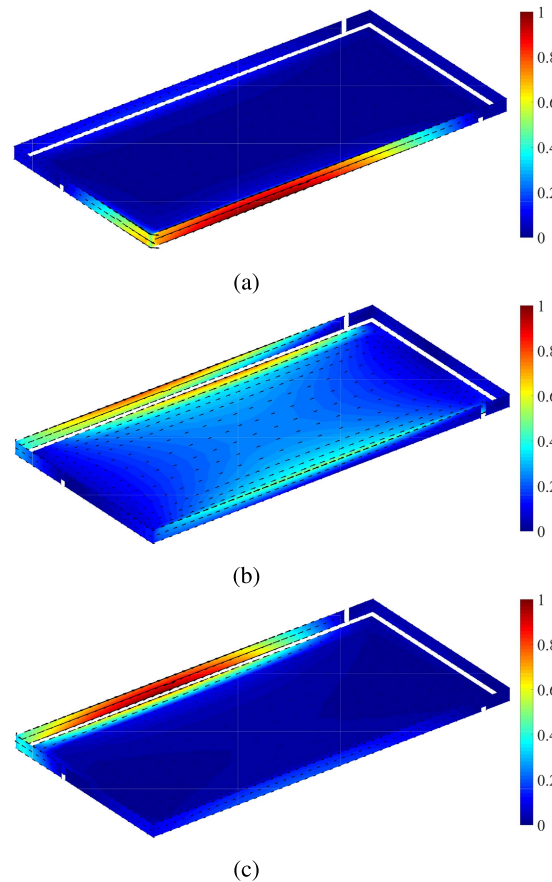

Fig. 3. Electric currents of the modes (a) B1 at 770 MHz, (b) B2 at 900 MHz, and (c) B3 at 885 MHz with normalized magnitudes.

modes due to the L-shaped sections of the rim, whereas mode B2 is dominated by the first fundamental ground plane mode having nonzero current on the rim too.

C. Metal-Rim Antenna With the Hand

Next, we add the hand to the model, as shown in Fig. 1. As material parameters for the hand, we use frequency-dependent complex permittivity [30, Table C-3].
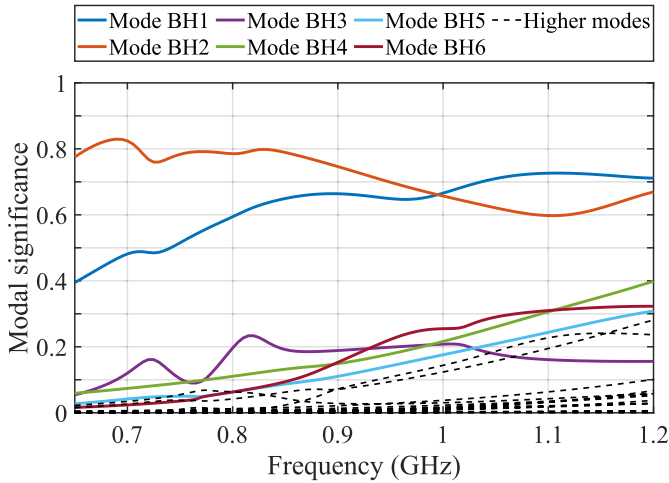
Fig. 4. Modal significances of 20 modes for the combined structure of Fig. 1.

Fig. 4 shows the modal significances of 20 modes for the combined antenna and hand structure. By comparing the results shown in Fig. 2 (the antenna without the hand) and Fig. 4 (the antenna with the hand), we observe several fundamental differences. First, the resonances of the modes are damped due to losses and σ_n does not reach value one. Second, there are only two significant modes, BH1 and BH2, while without the hand, we observe three significant modes B1, B2, and B3.

Current distributions in Fig. 5 show that mode BH2 is mostly due to the fundamental ground plane mode (corresponding to mode B2 without the hand). Modes BH1 and BH3 at 830 MHz agree pretty well with the modes of the L-sections of the rim (modes B1 and B3 without the hand). Looking at the results of Figs. 2 and 4 again, we see that mode B3, which has a very narrow resonance, is more damped due to losses than the other two. The results also show that modes B1 and B2 are mixed as the hand is added to the model. It is also important to note that the current distributions of the modes have rather strong frequency dependence. Study at a single frequency may not give a comprehensive picture of their behavior.

To further investigate the properties of the modes, Fig. 6 shows the modal efficiencies, defined in (7). Modes BH1 and BH2 contribute mostly on radiation, whereas mode BH3 has rather low η_n, indicating that it is either weaker radiator than the other two or it produces more losses.

Finally, we compare the antenna without and with the broken rim. Fig. 7(a) and (b) shows the modal coupling parameters κ_n for these two cases. Clearly, introducing the rim to the design leads to modes with smaller κ_n, indicating that currents on PEC dominate compared to the structure without the rim. The modal analysis results of this section suggest that a properly designed rim can have low coupling to the modes of the hand and, therefore, could be beneficial in reducing the user effect.

III. CM-BASED ANTENNA DESIGN

The antenna design is continued with the LB antenna based on the CMA results presented in Section II. The antenna
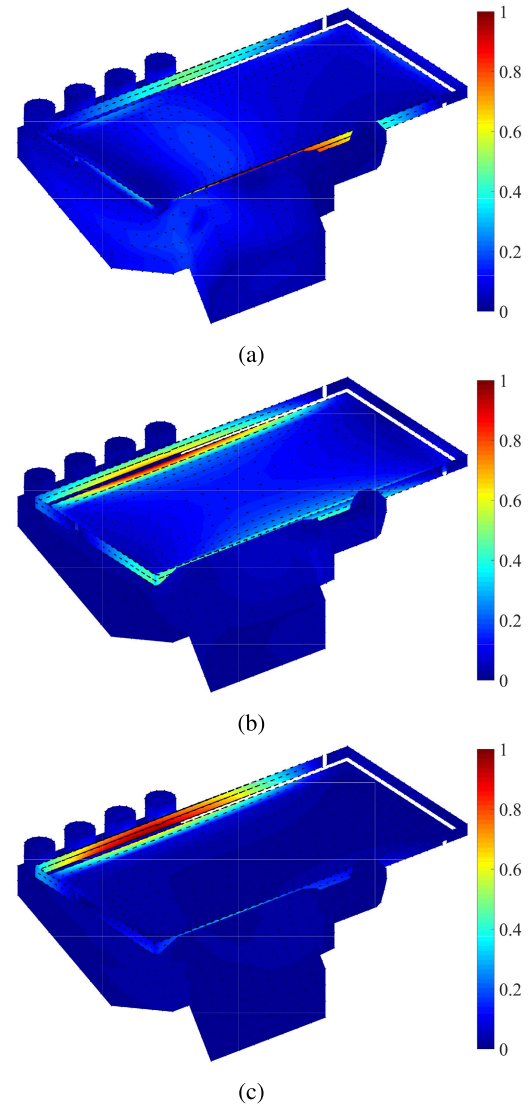

(a)

(b)

(c)

Fig. 5. Electric currents of the modes (a) BH1, (b) BH2, and (c) BH3, all at 830 MHz, with normalized magnitudes.
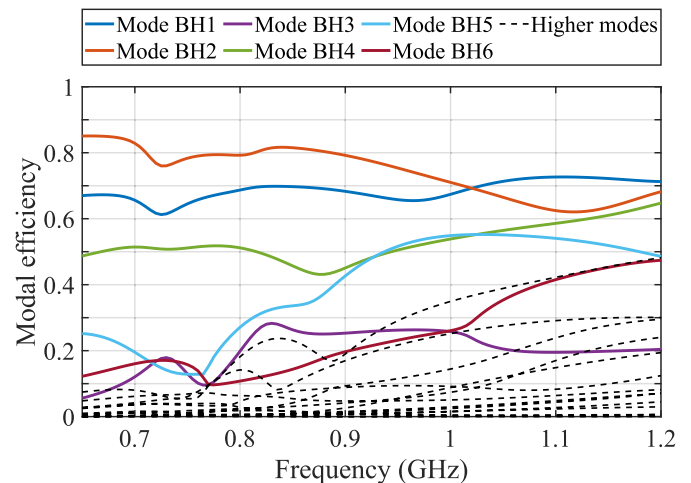

Fig. 6. Modal efficiencies of 20 modes for the combined structure of Fig. 1.

cluster technique is utilized to gain more freedom and adaptability in exciting and combining the desired modes of the
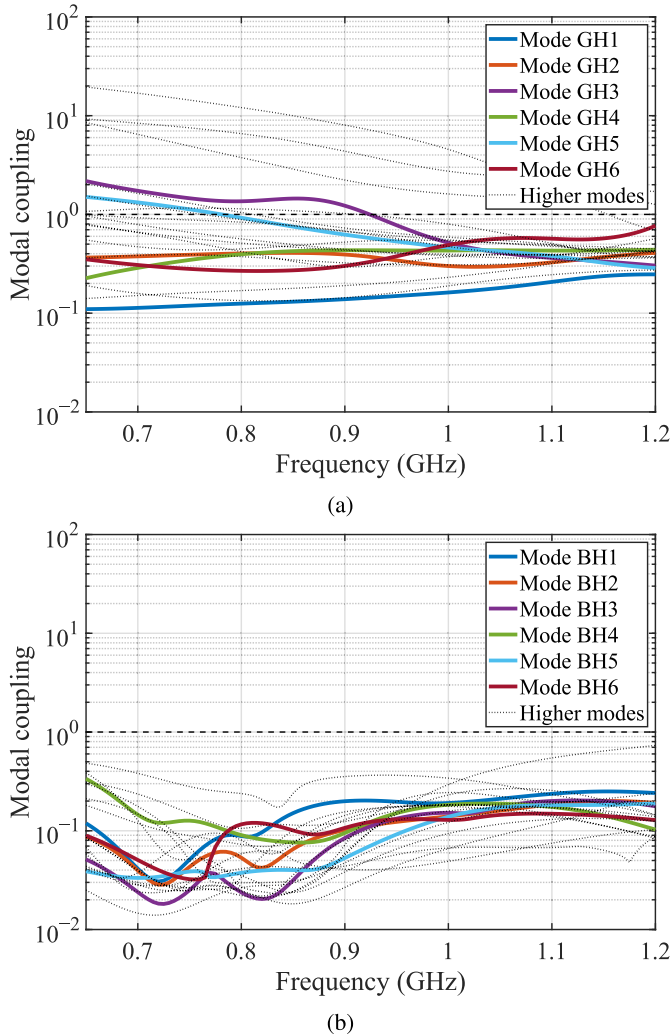
Fig. 7. Modal coupling parameters for (a) ground plane with the hand and (b) ground plane with the broken rim and the hand.

structure. Therefore, we proceed by introducing the required antenna cluster theory.

A. Antenna Cluster Technique

The antenna cluster technique [22], [23] uses several coupled antenna elements collaboratively combined with weighted feeding. The weighted feeding is a crucial part of the operation of antenna clusters. When the feeding signals have properly chosen amplitudes and phases, the signals fed to the ports couple to the other ports and the reflected signals partly cancel each other resulting in improvement in the radiation performance of the antenna cluster. Because these optimal feeding weights change with frequency, the cluster can be tuned to operate over a wide band by adjusting the weights accordingly.

An antenna cluster fed with complex feeding weights **a** has total efficiency of

$$\eta = \frac{\mathbf{a}^H \mathbf{D} \mathbf{a}}{\mathbf{a}^H \mathbf{a}} \qquad (9)$$

where **D** is the radiation matrix calculated from the far-field radiation patterns $\mathbf{F}_i$ of the antenna elements as [31]

$$D_{ij} = \frac{1}{4\pi} \iint_{4\pi} \mathbf{F}_i \cdot \mathbf{F}_j^* \, d\Omega \qquad (10)$$

normalized so that D_{ii} equals the total efficiency of the ith antenna element. Because (9) is a Rayleigh quotient [22], [31], the feeding weights **a** that maximize the total efficiency at each frequency point can be calculated as the magnitudes and phases of the eigenvector corresponding to the largest eigenvalue of **D**

$$\eta_{\max} = \max\{\mathrm{eig}(\mathbf{D})\}. \qquad (11)$$

When the radiation matrix is calculated from the far-field patterns, all the losses of the system, including the matching component losses, ohmic losses of metal conductors, and material losses of dielectric materials, are properly considered [31].

B. CMA-Based LB Cluster Design

To excite the wanted modes of the broken metal rim, we design a set of exciting elements. Based on the current distributions of the modes in Fig. 5, we know that the current distributions have maxima along the long edges of the device. These modes can be excited with elements placed near the current maxima for both of the L-shaped sections of the rim. In addition, a third element is placed to the short edge near the palm of the hand. Due to the utilized cluster technique, this element can be designed to excite the rim modes, to control the coupling between the other two elements for improved cluster operation, or as a combination of these operation modes depending on which is the most beneficial for the operation of the cluster in this frequency band.

The exciting elements are simple rectangular metal plates placed between the ground plane and the metal rim. To achieve wider bandwidth, matching circuits are used for all three elements and an additional reactive loading is used for element 2. To optimize the operation of the three-element cluster, the antenna geometry, matching circuits, and optimal feeding weights need to be designed simultaneously. The important thing in the matching circuit design is to include both the feeding weight optimization and the optimization of the component values into the same procedure.

The matching circuits for the antenna cluster in a lossy environment are optimized using the following procedure. First, the far-field patterns of all elements are simulated with the user's hand. Next, the component values are optimized using some numerical optimization algorithms, for example, the genetic algorithm used in this work. For each iteration of the optimization process, a set of matching circuit components is generated. The effects of these components are then embedded into the radiation matrix **D** of (10) by weighting the far-field patterns based on the modified excitations [32]. From this new radiation matrix, the optimal feeding amplitudes and phases for each frequency point are found as the complex eigenvector corresponding to the largest eigenvalue. The minimum total efficiency over the target band determined
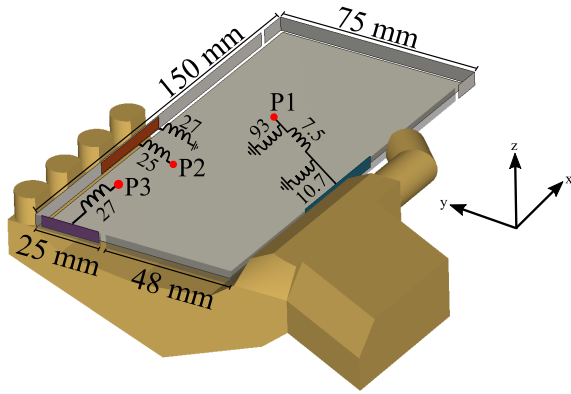
Fig. 8.   Simulation model of the LB antenna with the hand and the optimized matching components. Inductance values are in nH.
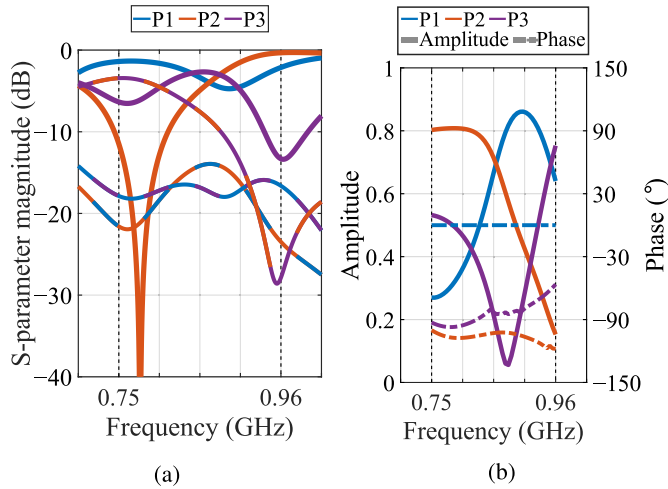

Fig. 9.   (a) S-parameters and (b) excitation signals of cluster elements in the LB. For the S-parameters, solid lines are reflection coefficients and interleaved dashed lines show coupling parameters between ports denoted by the colors.
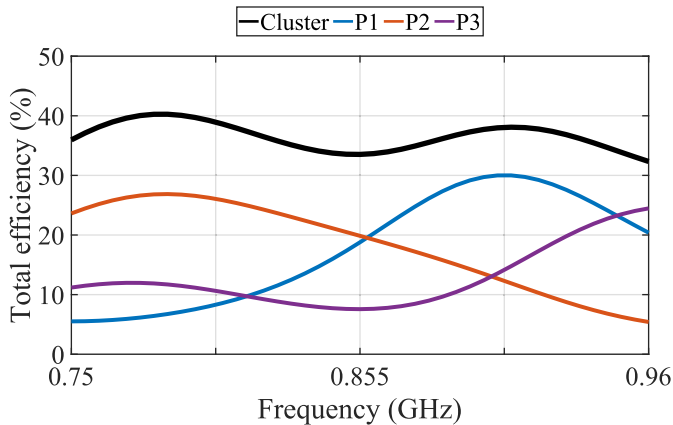

Fig. 10.   Total efficiencies of the individual antenna elements and the entire antenna cluster with optimal weights in the LB.

from (9) is then used as the optimization goal. Then, new iterations of the matching circuit components are generated by the optimization algorithm, and finally, the circuit giving the highest efficiency is chosen.

Fig. 8 shows the antenna structure, the port configuration, and the optimized matching circuits. The S-parameters of the LB antenna cluster elements and the optimal feeding

amplitudes and phases are shown in Fig. 9, and the total efficiencies of the individual elements and the antenna cluster are shown in Fig. 10. The results illustrate the operation principle of the antenna cluster. Elements 1 and 2 are mainly used to cover the higher and lower parts of the band, respectively, whereas the third element is used more as a supporting element. As can be seen from the results of Figs. 9 and 10, the efficiency and the feeding signal amplitude of the third element are generally lower than those of elements 1 and 2. Its main role is to enhance the operation of the antenna cluster by affecting the coupling between the elements, which is known to have a large impact on the antenna cluster operation [33].

The results of Figs. 9 and 10 demonstrate the benefits achieved with the antenna cluster technique. By combining the operation of several modes excited collaboratively with multiple coupled elements, we can cover wider frequency band with better performance than could be achieved with traditional single-feed solutions.

C. CMA Verification

The feeding elements and the reactive loadings designed in Section III-B might have an effect on the CMs. To see the contribution of each mode on the total solution, we compute the modal expansion coefficients c_n of the modes as in (5) with the feeding elements and matching components included in the analysis [6], i.e., using the structure and circuits given in Fig. 8.

Fig. 11 shows the modal expansion coefficients c_n for each of the three feeding ports. When the excitation is on port 1, the modes that have the strongest contribution on the modal expansion around 940 MHz are MH1–MH4. As the excitation is on port 2, modes MH1 and MH2 have the strongest contribution to the modal expansion around 810 MHz. Having the excitation on port 3, we recognize that the modal expansion coefficients are relatively high around the same frequencies as with ports 1 and 2, i.e., 810 and 940 MHz. In addition to modes MH1–MH3, at 960 MHz, also mode MH4 seems to be significant.

Next, we confirm that the original CMA results are still valid and that we have succeeded to excite the desired modes properly. The feeding elements with tiny geometrical details tend to accumulate currents, and therefore, we prefer to study radiation patterns instead of the currents. Fig. 12 shows the radiation patterns of the relevant modes BH1–BH3 without the ports and the corresponding modes MH1–MH3 with the ports.

Clearly, modes BH2 and MH2 have similar nearly symmetric radiation patterns. Also, the patterns of modes BH1 and MH1 and BH3 and MH3 have similar characteristics. We also note that the strongest radiation of mode BH1 is directed downward, toward the hand, whereas mode MH1 radiates upward away from the hand. We may conclude that the proposed feeding system has excited the wanted radiating modes properly.

IV. COMPLETE ANTENNA SYSTEM DESIGN AND RESULTS

After the LB antenna cluster operation has been designed and verified in Sections III-B and III-C, the complete antenna
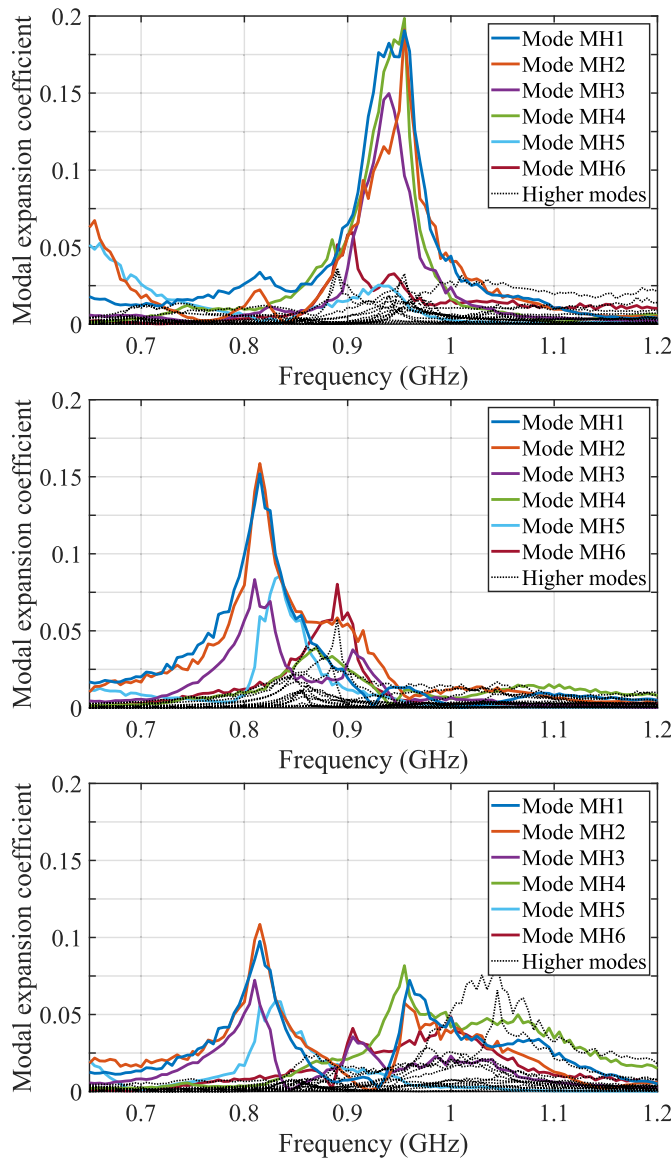
Fig. 11. Modal expansion coefficients for the proposed multiport antenna as excitations are at port 1 (top), port 2 (middle), and port 3 (bottom).
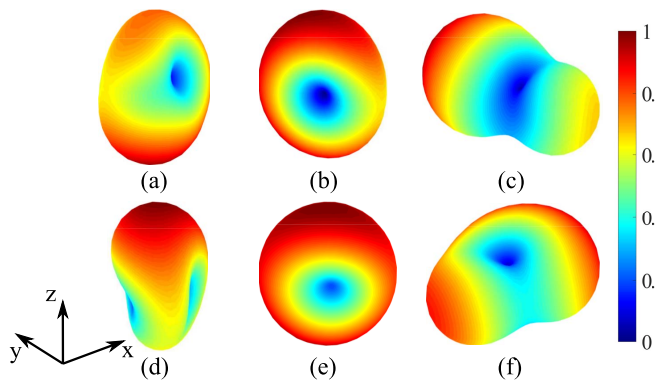

Fig. 12. Normalized radiation patterns of modes. (a) BH1, (b) BH2, (c) BH3, (d) MH1, (e) MH2, and (f) MH3, all at 830 MHz.

system is designed based on these results. For better correspondence between the simulations and the measurements, the simplified hand model used in the CMA for reduced

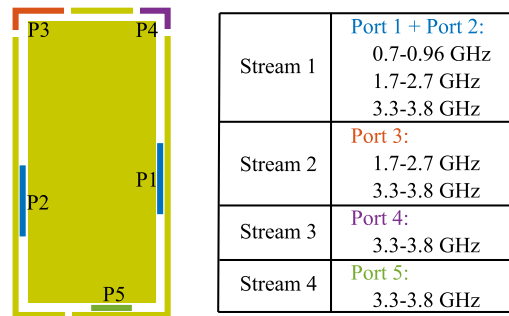|	
Stream 1	**Port 1 + Port 2:** 0.7–0.96 GHz 1.7–2.7 GHz 3.3–3.8 GHz
Stream 2	**Port 3:** 1.7–2.7 GHz 3.3–3.8 GHz
Stream 3	**Port 4:** 3.3–3.8 GHz
Stream 4	**Port 5:** 3.3–3.8 GHz

Fig. 13. Placement of the antenna elements and the frequency bands they cover in the complete antenna system.

computational complexity is changed for a standardized hand model similar to the actual hand phantom used in the measurements [30, A.1.3].

A. Design of Complete Antenna System

The complete antenna system is designed to cover the following frequency bands: 700–960 MHz LB with one multiport antenna, 1700–2700 MHz MHB with two MIMO antennas, and 3300–3800 MHz HB with four MIMO antennas. Fig. 13 shows how the feeding elements for ports 1, 2, and 5 are placed with respect to the L-shaped sections of the broken rim and how sections of the U-shaped part of the rim are excited with ports 3 and 4. Also, the covered frequency bands for each port are shown. To avoid confusion with the port numbering due to the multifeed antenna cluster of ports 1 and 2, we refer to the results of the MIMO antennas as data streams 1–4.

The antennas are designed using a Rogers RO4003C substrate material. The rim is assembled from four separate PCBs that have the metal rim printed on the outer side and the feeding elements on the inner side. These PCBs are attached to the main PCB and connected to each other at the corners. Because the exciting elements need to be placed close to the metal rim, 0.2 mm thickness is used for these, whereas the thickness of the main PCB is 0.8 mm.

The antenna cluster utilizing the combined operation of the two L-shaped sections of the lower part of the rim is based on the simplified model designed in Section III-B. Because the results of the antenna cluster showed that the third element is mainly used as a supporting element controlling the coupling between the first two elements, it is not used as an active element in this cluster in the final design. Instead, it is used as a separate MIMO antenna operating at the 3.3–3.8 GHz HB frequencies. Therefore, port 3 in Fig. 8 corresponds now to port 5 in Fig. 13. When all three elements are properly designed simultaneously, the third element can be used in the LB frequencies to support the antenna cluster of ports 1 and 2 and as an individual antenna in the HB frequencies without negatively affecting the cluster operation. All the elements have a matching circuit for feeding and a reactively loaded grounding strip at the end of the element, as shown in Fig. 14. The matching networks and the detailed dimensions and locations of the elements are optimized so that the cluster can cover all three main bands and the third element can cover the HB.
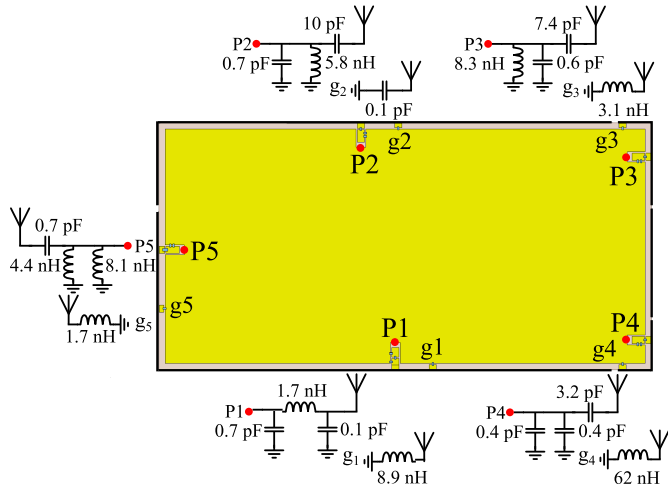
Fig. 14. Port configuration and realized matching circuits for the proposed antenna.

TABLE I
DIMENSIONS OF THE PROPOSED ANTENNA

Parameter	L_1	L_2	L_3	L_4	L_5	a
Value (mm)	35	35	25	15	20	2
Parameter	d_1	d_2	d_3	d_4	d_5	d_6
Value (mm)	49.5	17.3	24.8	39	10	33
Parameter	fd_1	fd_2	fd_3	fd_4	h_1	h_2
Value (mm	21	21	13.1	4,4	7	2.7
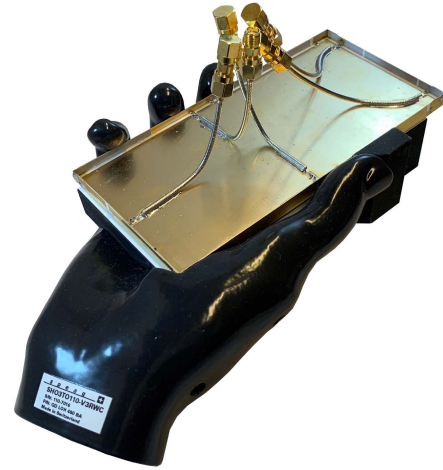
Fig. 16. Manufactured and measured prototype with the hand phantom.
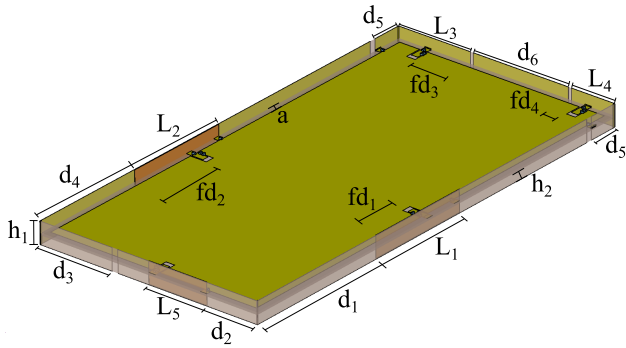

Fig. 15. Proposed antenna structure.

The rest of the required MHB and HB MIMO antennas are realized in the smaller U-shaped section of the rim in the upper end of the device. Because of the strictly limited volume and section of the rim available for these antennas, the design can be done without the need for a rigorous mode-based analysis. For this, the U-shaped section is further divided into three pieces: two sections in the corners and a piece of the rim in the middle. Because the modes studied in Section II have low currents in this part of the rim, this modification does not significantly affect the operation of the other antenna elements.

The corner elements are used as bent inverted-F-type antennas in the higher frequency bands. By reactively grounding the elements on the long edge of the ground plane right next to the cuts in the rim and by optimizing the distance of the feeding strip from the corner of the ground plane on the short edge, the larger element can be designed to cover both the 1.7–2.7 GHz MHB and the 3.3–3.8 GHz HB. Similarly, the smaller element is designed to cover only the HB. The feeding and grounding strips from the main PCB are directly connected to the rim PCB with vias connecting the inner side of the PCB and the metal rim on the outer side.

The realized matching circuit topologies and component values for all antennas are presented in Fig. 14. The final proposed antenna structure and the details of the dimensions are shown in Fig. 15 and Table I, respectively.

B. Results

A prototype of the proposed antenna is manufactured and measured. The measurements are performed with a Speag SHO3TO110-V3RWC hand phantom that is fully compliant with the CTIA standard [30]. The antenna prototype and the hand phantom are shown in Fig. 16. In addition to total efficiency, several other factors, such as coupling between the elements and correlation of the radiation patterns, affect the total performance of the antenna system. To take these factors into account and to more conveniently present the performance with a single figure of merit, we also study the ergodic capacities calculated from the simulated and measured far-field patterns using the method presented in [34]. All the capacity results presented in this work have been calculated using 10^4 channel realizations and SNR = 20 dB.

The far-field patterns of the antenna elements are measured individually by terminating the rest of the ports with 50 Ω loads. The patterns are then used to calculate the optimal feeding weights for the antenna cluster using (10) and (11). The cluster performance is calculated numerically from the combined radiation patterns. In a complete system, the feeding weights for the antenna cluster elements could be realized with multichannel transceiver integrated circuits.

The measured scattering parameters with the hand phantom are shown in Fig 17. The feeding weights for the antenna cluster are shown in Fig. 18. In the LB and MHB, the two elements are used collaboratively by changing the amount of power fed to each element and by adjusting the phase difference. In the HB, element 2 is in resonance and all the power is fed to port 2. Because port 1 is not used in the HB, port 5 can be used there without causing deterioration of
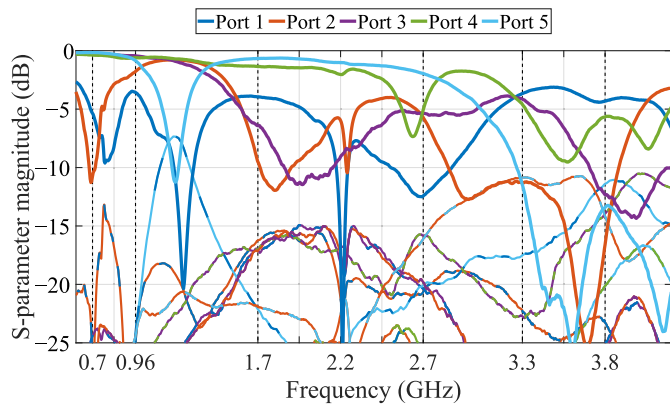
Fig. 17. Measured S-parameters with the hand phantom. Solid lines are reflection coefficients and interleaved dashed lines show coupling parameters between ports denoted by the colors.
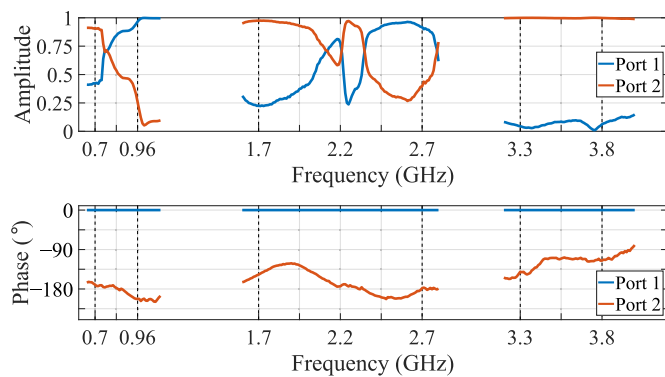

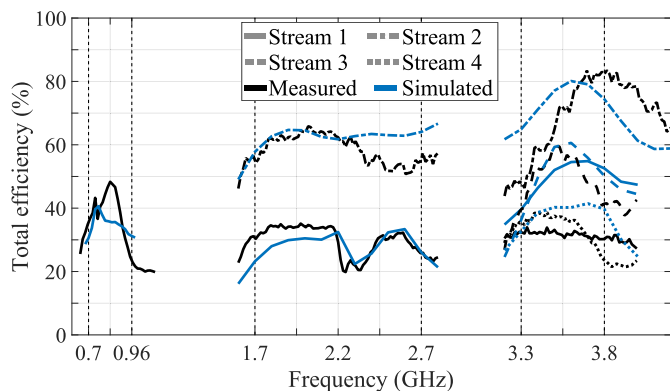Fig. 18. Feeding weights of ports 1 and 2 of the antenna cluster.

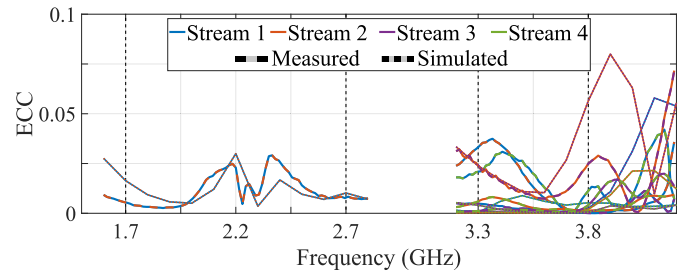Fig. 19. Measured and simulated total efficiencies with the hand phantom.

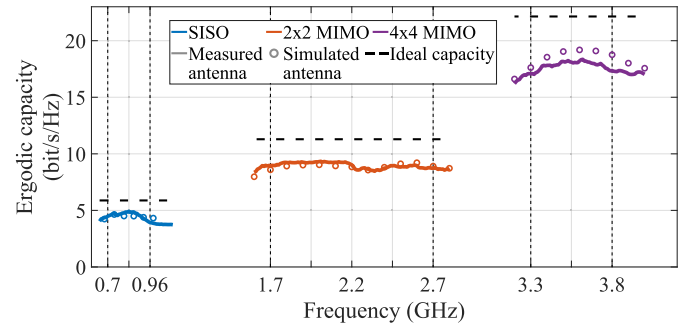Fig. 20. Measured and simulated ECCs with the hand phantom.

Fig. 21. MIMO capacities calculated using measured and simulated radiation patterns with the hand phantom.

maximum that could be achieved with 100 % efficient antennas having zero correlation. The correlation results show that all MIMO antennas have ECCs well below 0.5, which is traditionally considered as low correlation. The capacity results show that compared to the ideal capacities, the proposed antenna design achieves good results even though the device is being held by the user. Around 80 % of the ideal capacity is reached in all bands.

C. Further Analysis and Discussion

In practical smartphones, the components, such as the battery and the display panel, can affect the operation of the antennas. To study this, we use the simulation model shown in Fig. 22 with aluminum battery and display panel modeled with aluminum screen backplate and a glass ($\varepsilon_r = 5$ and $\tan\delta = 0.02$) panel. Simulated capacities with the user's hand with and without the components are shown in Fig. 22. In addition, the performance with the left hand holding the device and the device in free space without the hand is shown here. The results demonstrate that the components have only a minimal effect on the operation of the antennas.

The results of Fig. 22 show that the grip has only a minor effect and that the proposed antenna performs equally well with the user as in free space. This proves that the proposed method is effective in designing hand-immune antennas. In comparison, antennas designed with traditional methods might perform better in free-space conditions, but their operation is practically always severely degraded in a realistic usage scenario with the user.

A comparison between the proposed design and other published designs with the user is shown in Table II. The two clearance values are those along the short edge and the long edge of the device, respectively. The proposed design has extremely small ground clearance and it can cover all of

performance due to the elements placed to the same section of the rim.

The measured and simulated total efficiencies with the hand are presented in Fig. 19. Some antenna measurements show a small frequency shift compared to the simulations, but in general, there is a good agreement between the simulations and the measurements. In the LB, 30–48 % efficiency is achieved, 20–65 % efficiency is achieved in the MHB, and 24–83 % efficiency is achieved in the HB.

The envelope correlation coefficients (ECCs) of the MIMO antennas are shown in Fig. 20 and the ergodic capacities in Fig. 21. The ideal capacities for each MIMO order are also shown for comparison. These values correspond to the
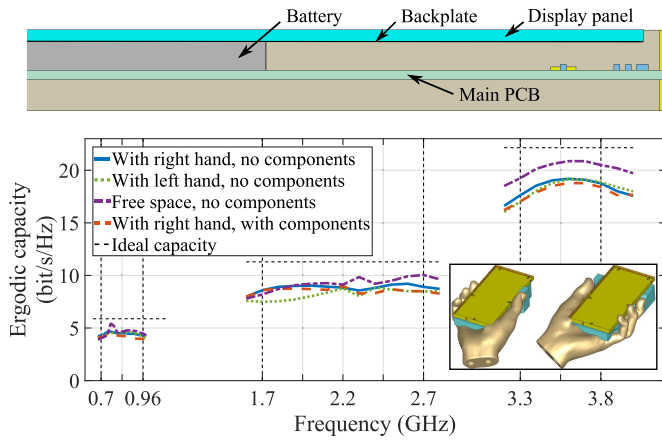
Fig. 22. Simulation model for the smartphone components and comparison of the simulated MIMO capacities in different scenarios. Inset: difference between the right and left hand grips.

TABLE II

COMPARISON OF THE PROPOSED DESIGN WITH OTHER PUBLISHED DESIGNS WITH USER EFFECT

Antenna	Clearance (mm)	Frequency bands (GHz)	MIMO order	Efficiency (%)
Proposed	**2/2**	**LB: 0.7–0.96**	**1**	**30–48**
		MHB: 1.7–2.7	**2**	**20–65**
		HB: 3.3–3.8	**4**	**24–83**
[35]	8/2	HB: 3.4–3.6	8	2–73
[13]	5/2	LB: 0.824–0.96	1	15–20
		MHB: 1.7–2.7	1	14–30
[18]	6+2*/2	LB: 0.824–0.96	1	23–25
		MHB: 1.7–2.7	1	25–38
[36]	2/2	LB: 0.82–0.96**	2	14–32
		MHB: 1.7–2.7	2	16–57
[37]	11/0	LB: 0.7–0.96	1	33–46
		MHB: 1.7–2.7	1	28–63
[17]	2/3.5	LB: 0.86–0.98	2	12–25
[38]	8/1	LB: 0.824–0.96	1	23–27
		MHB: 1.7–2.7	1	33–41

* bottom + top

** Low-band results with user presented for this frequency range only

the LB, MHB, and HB, with two and four MIMO antennas in the MHB and HB, respectively. Compared with the other designs, the proposed design has the smallest ground clearance and the best performance considering the number of antennas and the covered frequency bands. For example, covering the LB from 700 MHz with better than 30 % efficiency with the user has required more than 10 mm of clearance in the previous designs. The comparison shows that very good performance has been achieved.

V. CONCLUSION

The design process of a hand-immune mobile antenna system has been presented. The effect of the user's hand is considered in a special CMA method developed for lossy structures. We have shown that a metal rim around the phone chassis introduces additional modes that couple less to the lossy dielectric parts, such as user's hand, than the modes

present in the chassis only. Because of the low coupling to nearby dielectric bodies, these modes are less sensitive to the user effect. The resonance frequencies of the rim modes can be adjusted by properly dividing the rim into sections. Combined with advanced adaptive feeding arrangement based on the antenna cluster technique, we were able to efficiently excite the user-insensitive modes, improving the performance of the antenna and making it almost completely immune to the presence of the user. An antenna system covering the 700–960 MHz LB, 1700–2700 MHz MHB, and 3300–3800 MHz HB with one, two, and four MIMO antennas, respectively, has been designed, manufactured, and measured with results showing good performance.

REFERENCES

[1] R. Khan, A. A. Al-Hadi, and P. J. Soh, "Recent advancements in user effect mitigation for mobile terminal antennas: A review," *IEEE Trans. Electromagn. Compat.*, vol. 61, no. 1, pp. 279–287, Feb. 2019.

[2] Y. Chen and C. Wang, *Characteristic Modes–Theory and Applications in Antenna Engineering*. Hoboken, NJ, USA: Wiley, 2015.

[3] W. Wu and Y. P. Zhang, "Analysis of ultra-wideband printed planar quasi-monopole antennas using the theory of characteristic modes," *IEEE Antennas Propag. Mag.*, vol. 52, no. 6, pp. 67–77, Dec. 2010.

[4] R. Martens, E. Safin, and D. Manteuffel, "Inductive and capacitive excitation of the characteristic modes of small terminals," in *Proc. Loughborough Antennas Propag. Conf.*, Nov. 2011, pp. 1–4.

[5] A. Krewski, W. L. Schroeder, and K. Solbach, "Multi-band 2-port MIMO LTE antenna design for laptops using characteristic modes," in *Proc. Loughborough Antennas Propag. Conf. (LAPC)*, Nov. 2012, pp. 1–4.

[6] E. Safin and D. Manteuffel, "Manipulation of characteristic wave modes by impedance loading," *IEEE Trans. Antennas Propag.*, vol. 63, no. 4, pp. 1756–1764, Apr. 2015.

[7] T. Hadamik, R. Martens, and D. Manteuffel, "MIMO antenna concept based on Characteristic Modes for indoor base stations," in *Proc. 9th Eur. Conf. Antennas Propag. (EuCAP)*, Apr. 2015, pp. 1–2.

[8] M. Bouezzeddine and W. L. Schroeder, "Design of a wideband, tunable four-port MIMO antenna system with high isolation based on the theory of characteristic modes," *IEEE Trans. Antennas Propag.*, vol. 64, no. 7, pp. 2679–2688, Jul. 2016.

[9] C. Deng, Z. Feng, and S. V. Hum, "MIMO mobile handset antenna merging characteristic modes for increased bandwidth," *IEEE Trans. Antennas Propag.*, vol. 64, no. 7, pp. 2660–2667, Jul. 2016.

[10] F. H. Lin and Z. N. Chen, "Low-profile wideband metasurface antennas using characteristic mode analysis," *IEEE Trans. Antennas Propag.*, vol. 65, no. 4, pp. 1706–1713, Apr. 2017.

[11] D. Wen, Y. Hao, H. Wang, and H. Zhou, "Design of a wideband antenna with stable omnidirectional radiation pattern using the theory of characteristic modes," *IEEE Trans. Antennas Propag.*, vol. 65, no. 5, pp. 2671–2676, May 2017.

[12] N. Mohamed Mohamed-Hicho, E. Antonino-Daviu, M. Cabedo-Fabres, and M. Ferrando-Bataller, "Designing slot antennas in finite platforms using characteristic modes," *IEEE Access*, vol. 6, pp. 41346–41355, 2018.

[13] Y. Liu, J. Zhang, A. Ren, H. Wang, and C.-Y.-D. Sim, "TCM-based hepta-band antenna with small clearance for metal-rimmed mobile phone applications," *IEEE Antennas Wireless Propag. Lett.*, vol. 18, no. 4, pp. 717–721, Apr. 2019.

[14] D. Wen, Y. Hao, H. Wang, and H. Zhou, "Design of a MIMO antenna with high isolation for smartwatch applications using the theory of characteristic modes," *IEEE Trans. Antennas Propag.*, vol. 67, no. 3, pp. 1437–1447, Mar. 2019.

[15] Y. Liu, A. Ren, H. Liu, H. Wang, and C.-Y.-D. Sim, "Eight-port MIMO array using characteristic mode theory for 5G smartphone applications," *IEEE Access*, vol. 7, pp. 45679–45692, 2019.

[16] H. Li, Z. T. Miers, and B. K. Lau, "Design of orthogonal MIMO handset antennas based on characteristic mode manipulation at frequency bands below 1 GHz," *IEEE Trans. Antennas Propag.*, vol. 62, no. 5, pp. 2756–2766, May 2014.

[17] L. Qu, J. Jeon, D. Park, and H. Kim, "Antenna design based on quasi-degenerate characteristic modes of unbroken metal rim," *IET Microw., Antennas Propag.*, vol. 11, no. 15, pp. 2168–2173, 2017.

[18] C. Deng, Z. Xu, A. Ren, and S. V. Hum, "TCM-based bezel antenna design with small ground clearance for mobile terminals," *IEEE Trans. Antennas Propag.*, vol. 67, no. 2, pp. 745–754, Feb. 2019.

[19] I. Vasilev and B. K. Lau, "On user effects in MIMO handset antennas designed using characteristic modes," *IEEE Antennas Wireless Propag. Lett.*, vol. 15, pp. 758–761, 2016.

[20] P. Ylä-Oijala, H. Wallén, and S. Järvenpää, "Theory of characteristic modes for lossy structures: Formulation and interpretation of eigenvalues," *Int. J. Numer. Model., Electron. Netw., Devices Fields*, vol. 33, no. 2, p. e2627, Mar. 2020.

[21] P. Yla-Oijala, A. Lehtovuori, H. Wallen, and V. Viikari, "Coupling of characteristic modes on PEC and lossy dielectric structures," *IEEE Trans. Antennas Propag.*, vol. 67, no. 4, pp. 2565–2573, Apr. 2019.

[22] J.-M. Hannula, J. Holopainen, and V. Viikari, "Concept for frequency-reconfigurable antenna based on distributed transceivers," *IEEE Antennas Wireless Propag. Lett.*, vol. 16, pp. 764–767, 2017.

[23] J.-M. Hannula, T. Saarinen, J. Holopainen, and V. Viikari, "Frequency reconfigurable multiband handset antenna based on a multichannel transceiver," *IEEE Trans. Antennas Propag.*, vol. 65, no. 9, pp. 4452–4460, Sep. 2017.

[24] R. Luomaniemi, J.-M. Hannula, R. Kormilainen, A. Lehtovuori, and V. Viikari, "Unbroken metal rim MIMO antenna utilizing antenna clusters," *IEEE Antennas Wireless Propag. Lett.*, vol. 18, no. 6, pp. 1071–1075, Jun. 2019.

[25] R. Luomaniemi, J.-M. Hannula, R. Kormilainen, A. Lehtovuori, and V. Viikari, "User effect on antenna cluster based MIMO antenna," in *Proc. Antennas Propag. Conf. (APC)*, Nov. 2019, pp. 3–5.

[26] R. Luomaniemi, A. Salmi, A. Lehtovuori, and V. Viikari, "Reducing user effect on mobile antenna systems with antenna cluster technique," in *Proc. 14th Eur. Conf. Antennas Propag. (EuCAP)*, Mar. 2020, pp. 1–4.

[27] P. Yla-Oijala, "Generalized theory of characteristic modes," *IEEE Trans. Antennas Propag.*, vol. 67, no. 6, pp. 3915–3923, Jun. 2019.

[28] R. Harrington and J. Mautz, "Theory of characteristic modes for conducting bodies," *IEEE Trans. Antennas Propag.*, vol. 19, no. 5, pp. 622–628, Sep. 1971.

[29] P. Yla-Oijala and H. Wallen, "Theory of characteristic modes for non-symmetric surface integral operators," *IEEE Trans. Antennas Propag.*, early access, Aug. 24, 2020, doi: 10.1109/TAP.2020.3017437.

[30] *Test Plan for Wireless Device Over-the-Air Performance*, CTIA, Washington, DC, USA, May 2015.

[31] J.-M. Hannula, T. O. Saarinen, A. Lehtovuori, J. Holopainen, and V. Viikari, "Tunable eight-element MIMO antenna based on the antenna cluster concept," *IET Microw., Antennas Propag.*, vol. 13, no. 7, pp. 959–965, Jun. 2019.

[32] S. Otto, S. Held, A. Rennings, and K. Solbach, "Array and multiport antenna farfield simulation using EMPIRE, MATLAB and ADS," in *Proc. Eur. Microw. Conf. (EuMC)*, Sep./Oct. 2009, pp. 1547–1550.

[33] J.-M. Hannula, A. Lehtovuori, R. Luomaniemi, T. O. Saarinen, and V. Viikari, "Beneficial interaction of coupling and mismatch in a two-antenna system," in *Proc. 13th Eur. Conf. Antennas Propag. (EuCAP)*, Mar./Apr. 2019, pp. 1–4.

[34] R. Tian, B. K. Lau, and Z. Ying, "Multiplexing efficiency of MIMO antennas," *IEEE Antennas Wireless Propag. Lett.*, vol. 10, pp. 183–186, 2011.

[35] H. Xu, S. S. Gao, H. Zhou, H. Wang, and Y. Cheng, "A highly integrated MIMO antenna unit: Differential/Common mode design," *IEEE Trans. Antennas Propag.*, vol. 67, no. 11, pp. 6724–6734, Nov. 2019.

[36] J. Choi, W. Hwang, C. You, B. Jung, and W. Hong, "Four-element reconfigurable coupled loop MIMO antenna featuring LTE full-band operation for metallic-rimmed smartphone," *IEEE Trans. Antennas Propag.*, vol. 67, no. 1, pp. 99–107, Jan. 2019.

[37] M. Stanley, Y. Huang, H. Wang, H. Zhou, Z. Tian, and Q. Xu, "A novel reconfigurable metal rim integrated open slot antenna for octa-band smartphone applications," *IEEE Trans. Antennas Propag.*, vol. 65, no. 7, pp. 3352–3363, Jul. 2017.

[38] Y. Liu, Y.-M. Zhou, G.-F. Liu, and S.-X. Gong, "Heptaband Inverted-F antenna for metal-rimmed mobile phone applications," *IEEE Antennas Wireless Propag. Lett.*, vol. 15, pp. 996–999, 2016.

Rasmus Luomaniemi (Graduate Student Member, IEEE) was born in Salo, Finland, in 1994. He received the B.Sc. (Tech.) and M.Sc. (Tech.) degrees (Hons.) in electrical engineering from Aalto University, Espoo, Finland, in 2016 and 2018, respectively, where he is currently pursuing the D.Sc. (Tech.) degree.

Since 2014, he has been with the Department of Electronics and Nanoengineering, School of Electrical Engineering, Aalto University. His current research interests include multiple-input–multiple-output MIMO antennas for mobile devices and multiport antennas.

Mr. Luomaniemi was a recipient of the Second Prize in the IEEE AP-S Student Design Contest as a part of the Team Aalto ELEC, in 2016.

Pasi Ylä-Oijala received the M.Sc. and Ph.D. degrees in applied mathematics from the University of Helsinki, Helsinki, Finland, in 1992 and 1999, respectively.

From 2004 to 2010, he was pointed as an Academy Research Fellow by the Academy of Finland. He is currently a Staff Scientist with the Department of Electronics and Nanoengineering, Aalto University, Espoo, Finland. His fields of interest include stable and efficient integral equation-based methods in computational electromagnetics, theory and application of characteristic modes, and electromagnetic modeling of complex material structures.

Anu Lehtovuori received the M.Sc. (Tech.) and Lic.Sc. (Tech.) degrees from the Helsinki University of Technology, Espoo, Finland, in 2000 and 2003, respectively, and the D.Sc. (Tech.) degree from Aalto University, Espoo, in 2015, all in electrical engineering.

She is currently a University Lecturer in circuit theory with the School of Electrical Engineering, Aalto University. Her current research interests include electrically small antennas, multiport antennas, and design of antennas for mobile devices.

Ville Viikari (Senior Member, IEEE) was born in Espoo, Finland, in 1979. He received the Master of Science (Tech.) and Doctor of Science (Tech.) (Hons.) degrees in electrical engineering from the Helsinki University of Technology (TKK), Espoo, in 2004 and 2007, respectively.

From 2001 to 2007, he was with the Radio Laboratory, TKK, where he studied antenna measurement techniques at submillimeter wavelengths and antenna pattern correction techniques. From 2007 to 2012, he was a Research Scientist and a Senior Scientist with the VTT Technical Research Center, Espoo, where his research included wireless sensors, RFID, radar applications, MEMS, and microwave sensors. He is currently an Associate Professor and the Deputy Head of the department, School of Electrical Engineering, Aalto University, Espoo. His current research interests include antennas for mobile networks, RF-powered devices, and antenna measurement techniques.

Dr. Viikari was a recipient of the Young Researcher Award of the Year 2014 presented by the Finnish Foundation for Technology Promotion, the IEEE Sensors Council 2010 Early Career Gold Award, the 2008 Young Scientist Award of the URSI XXXI Finnish Convention on Radio Science, Espoo, and the Best Student Paper Award of the annual symposium of the Antenna Measurement Techniques Association, Newport, RI, USA (October 30–November 4, 2005). He has served as the Chair for the Technical Program Committee of the ESA Workshop on Millimeter-Wave Technology and Applications and the Global Symposium on Millimeter Waves (GSMM) in 2011 and 2016, Espoo.